Strain accumulation in sand due to drained uniaxial cyclic loading

T. Wichtmann, A. Niemunis & Th. Triantafyllidis
Institute of Soil Mechanics and Foundation Engineering, Ruhr-University Bochum

ABSTRACT: A constitutive model for the material behaviour of sand under cyclic loading is presented. The explicit formulas predicting the accumulation of strain under drained conditions and pore water pressure development under undrained conditions are derived on the basis of cyclic triaxial tests and cyclic multiaxial direct simple shear (CMDSS) tests. This paper presents the results of numerous triaxial tests with uniaxial cyclic loading, i.e. only the vertical stress component was varied. The influence of strain amplitude, average stress and initial density on the intensity of accumulation and the cyclic flow rule is pointed out. The results of cyclic triaxial tests with a simultaneous variation of lateral and vertical stresses as well as the experiments with the CMDSS device are presented in the companion paper, Wichtmann et al. (2004b).

1 INTRODUCTION

Since the stress - strain response is not perfectly reversible cyclic loading leads to an accumulation of strain in soils under drained conditions and to a rise of pore water pressure if drainage is prevented. These cumulative phenomena may lead to large settlements endangering the serviceability of structures (e.g. foundations of magnetic levitation train). In the undrained case cyclic loading may generate high pore pressures and even lead to a loss of the bearing capacity of a foundation (e.g. foundations of off-shore wind power plants). The cyclic accumulation may also be helpful for the mechanical densification of artificial poured soil deposits.

For an accurate prediction of settlements or pore water generation under cyclic loading an appropriate constitutive model is needed. Concerning the calculation of the accumulation due to cyclic loading two strategies can be distinguished. In the *implicit* method each cycle is incrementally calculated using a high quality constitutive model for monotonic loading. The accumulation results from the fact that the loops are not perfectly closed. However, small systematic errors of the material model or the integration routine accumulate with each cycle and may reach the magnitude of the physical accumulation. Thus, the implicit approach is not suitable for higher numbers of cycles ($N > 50$).

Explicit (N-type) models predict the accumulation due to a bunch of ΔN cycles within a single increment directly by empirical formulas. A representative cycle is calculated incrementally in order to determine the strain amplitude from the strain path during this cycle. The strain amplitude is the basic parameter of the explicit model. After several hundreds of cycles an implicit calculation (so-called *control* cycle) can be inserted in order to consider changes in the elastic material behaviour due to void ratio changes or stress redistributions.

Our material model is explicit. The empirical formulas were derived on the basis of numerous cyclic triaxial tests and cyclic multiaxial direct simple shear (CMDSS) tests. This paper deals with the influence of the average stress $\boldsymbol{\sigma}^{\mathrm{av}}$, the strain amplitude $\varepsilon^{\mathrm{ampl}}$ and the initial density e on the intensity and direction (flow rule) of accumulation. The incorporation of these effects in the material model is presented. In the cyclic triaxial tests performed for this purpose only the vertical stress component was varied.

A special attention is given to isotropic compression cycles. In the literature one may find that their effect can be disregarded. The companion paper (Wichtmann et al. 2004b) presents cyclic triaxial tests with a simultaneous variation of the vertical and lateral stress components, thus different ratios of deviatoric and volumetric portion of the strain loop and their contribution to the accumulation process were studied. The influence of the shape of the strain loop and the effect of changes of the strain polarization during cyclic loading were studied in the CMDSS tests. The companion paper also summarizes the results of these tests and the incorporation of the observed material behaviour in the constitutive model.

A detailed review of literature concerning cyclic laboratory tests on non-cohesive materials is given by Wichtmann et al. (2004a).

2 NOTATION

For an arbitrary state variable $\sqcup$ we define its average value $\sqcup^{\text{av}}$ upon a cycle in such way that $\sqcup^{\text{av}}$ is the center of the smallest sphere that encompasses all states $\sqcup^{(i)}$ of a given cycle. The average value $\sqcup^{\text{av}}$ should not be mixed up with the *mean* value $\frac{1}{n}\sum_{i=1}^{n}\sqcup^{(i)}$. The amplitude is defined as $\sqcup^{\text{ampl}} = \max \| \sqcup^{(i)} - \sqcup^{\text{av}} \|$. A more elaborated definition of a multiaxial amplitude (including polarization and openness of the strain loop) is given in Niemunis et al. (2004).

In this paper the effective Cauchy stress $\boldsymbol{\sigma}$ is used with the Roscoe invariants $p = tr(\boldsymbol{\sigma})/3$ and $q = \sqrt{3/2}\,\|\boldsymbol{\sigma}^*\|$ and the conjugated strain rates $\dot{\varepsilon}_v$ and $\dot{\varepsilon}_q$ such that $p\,\dot{\varepsilon}_v + q\,\dot{\varepsilon}_q = \boldsymbol{\sigma} : \dot{\boldsymbol{\varepsilon}}$. Using the so-called explicit description of the cumulative behaviour of soil the word "rate" means the derivative with respect to the number of cycles N, that is $\dot{\sqcup} = \partial \sqcup / \partial N$. $\sqcup^*$ denotes the deviatoric part of $\sqcup$. Sometimes we also use the isomorphic variables $P = \sqrt{3}\,p$, $Q = \sqrt{2/3}\,q$, $\dot{\varepsilon}_P = 1/\sqrt{3}\,\dot{\varepsilon}_v$ and $\dot{\varepsilon}_Q = \sqrt{3/2}\,\dot{\varepsilon}_q$ in order to preserve orthogonality in the invariant space. We denote the axial components of stress and strain with the index $\sqcup_1$ and the lateral components with $\sqcup_2$ and $\sqcup_3$. The Roscoe variables for the triaxial case are therefore $p = (\sigma_1 + 2\sigma_3)/3$ and $q = \sigma_1 - \sigma_3$ and the conjugated strain rates $\dot{\varepsilon}_v = \dot{\varepsilon}_1 + 2\dot{\varepsilon}_3$ and $\dot{\varepsilon}_q = 2/3\,(\dot{\varepsilon}_1 - \dot{\varepsilon}_3)$.

Stress obliquity may be expressed by $\eta = q/p$ or using the yield function $Y = -I_1 I_2 / I_3$ (I_i: basic invariants of stress tensor $\boldsymbol{\sigma}$) of Matsuoka and Nakai (1982) as

$$\bar{Y} = \frac{Y - 9}{Y_c - 9} \qquad Y_c = \frac{9 - \sin^2\varphi}{1 - \sin^2\varphi} \tag{1}$$

The critical friction angle is denoted by φ and the peak one as φ_p. The variables η and Y are interrelated via

$$Y = \frac{27(3+\eta)}{(3+2\eta)(3-\eta)} \tag{2}$$

The inclinations of the critical state line (see Fig. 1) are

$$M_c = \frac{6\,\sin\varphi}{3 - \sin\varphi}, \quad \text{and} \quad M_e = -\frac{6\,\sin\varphi}{3 + \sin\varphi} \tag{3}$$

for compression and extension and correspond to $\bar{Y} = 1$.

The average stress $\boldsymbol{\sigma}^{\text{av}}$ is superimposed with a cyclic part with amplitudes σ_1^{ampl} and σ_3^{ampl}. This paper presents exclusively tests where the lateral stress σ_3 was kept constant, i.e. $\sigma_3^{\text{ampl}} = 0$, corresponding to stress paths with an inclination of $\tan(\alpha)$ = 3 in the p - q - plane (see Fig. 1). For the description of the stress amplitude in such tests we use

$$\zeta = \sigma_1^{\text{ampl}} / p^{\text{av}} \ . \tag{4}$$

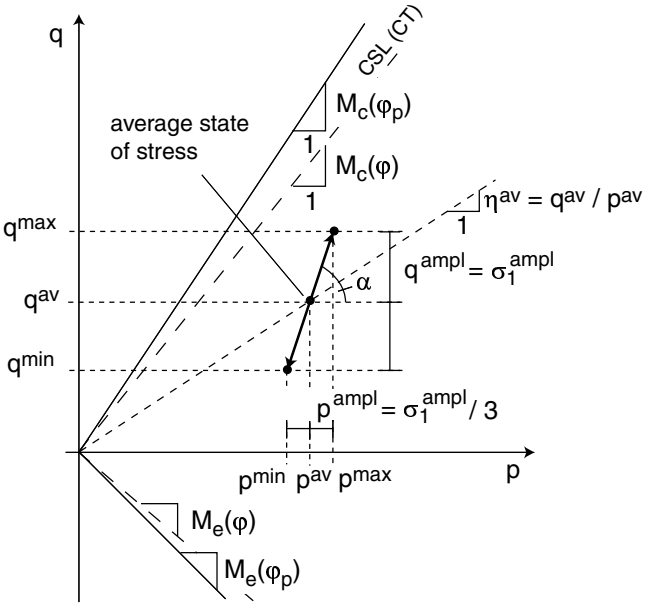

Figure 1. State of stress in a cyclic triaxial test

The strains under cyclic loading can be decomposed into a residual and a resilient portion denoted by the superscripts $\sqcup^{\text{acc}}$ and $\sqcup^{\text{ampl}}$, respectively. We abbreviate

$$\varepsilon^{\text{acc}} = \|\boldsymbol{\varepsilon}^{\text{acc}}\| = \int \dot{\boldsymbol{\varepsilon}}^{\text{acc}} \mathrm{d}N \tag{5}$$

For triaxial tests with $\boldsymbol{\sigma}^{\text{av}}$ = const. the direction of the accumulated strain is almost constant and therefore $\varepsilon^{\text{acc}} = \sqrt{(\varepsilon_1^{\text{acc}})^2 + 2(\varepsilon_3^{\text{acc}})^2}$. As a scalar measure of the direction of accumulation the strain ratio

$$\omega = \varepsilon_v^{\text{acc}} / \varepsilon_q^{\text{acc}} \tag{6}$$

is used, wherein $\varepsilon_v^{\text{acc}}$ and $\varepsilon_q^{\text{acc}}$ are the cumulative volumetric and deviatoric strain components, respectively. The basic variable that dictates the rate of accumulation is chosen to be the strain amplitude. In the evaluation of the cyclic triaxial tests the deviatoric part of the strain amplitude was initially believed to be alone responsible for the accumulation. Therefore we define

$$\gamma^{\text{ampl}} = (\varepsilon_1 - \varepsilon_3)^{\text{ampl}} = \sqrt{\frac{3}{2}}\,(\boldsymbol{\varepsilon}^*)^{\text{ampl}} \tag{7}$$

This assumption turned out to be controversal. Recently the volumetric amplitude has been studied in Wichtmann et al. (2004b).

Specimen density is described by the density index $I_D = (e_{\max} - e)/(e_{\max} - e_{\min})$ with the maximum and minimum void ratios determined from standard tests.

3 MATERIAL MODEL

The purpose of the cyclic triaxial tests was to provide data for an explicit constitutive model which describes the phenomenon of cyclic accumulation. The general stress-strain relation has the form

$$\dot{\boldsymbol{\sigma}} \;=\; \mathsf{E} : (\dot{\boldsymbol{\varepsilon}} - \dot{\boldsymbol{\varepsilon}}^{\mathrm{acc}}) \tag{8}$$

wherein E denotes an elastic stiffness calculated for the given stress $\boldsymbol{\sigma}$. The rate of strain accumulation $\dot{\boldsymbol{\varepsilon}}^{\mathrm{acc}}$ is proposed to be

$$\begin{aligned} \dot{\boldsymbol{\varepsilon}}^{\mathrm{acc}} &= \dot{\varepsilon}^{\mathrm{acc}}\,\mathbf{m} \;=\; (\dot{\varepsilon}^{\mathrm{acc}\ A} + \dot{\varepsilon}^{\mathrm{acc}\ B})\,\mathbf{m} \\ &= f_{\mathrm{ampl}}\, f_p\, f_Y\, f_e\, f_\pi\, (\dot{f}_N^{\,A} + \dot{f}_N^{\,B})\,\mathbf{m} \end{aligned} \tag{9}$$

with the direction expressed by the unit tensor $\mathbf{m}$ (for triaxial tests $\omega = \sqrt{3/2}\ \mathrm{tr}\,\mathbf{m}/\|\mathbf{m}^*\|$ holds) and with the intensity $\dot{\varepsilon}^{\mathrm{acc}} = \|\dot{\boldsymbol{\varepsilon}}^{\mathrm{acc}}\|$. $\dot{\varepsilon}^{\mathrm{acc}}$ is proposed to be decomposed into a part $\dot{\varepsilon}^{\mathrm{acc}\ A}$ related to the structure of the material and a residual part $\dot{\varepsilon}^{\mathrm{acc}\ B}$ which becomes dominant for large numbers of cycles. The accumulated structural deformation $\varepsilon^{\mathrm{acc}\ A}$ is treated as a state variable enabling the calculation of subsequent packages of cycles with different amplitudes (see Niemunis et al. 2004 and Subsection 5.4).

The intensity of strain accumulation $\dot{\varepsilon}^{\mathrm{acc}}$ depends on the strain amplitude γ^{ampl}, the applied number of cycles N, the average stress $p^{\mathrm{av}}, \bar{Y}^{\mathrm{av}}$, the void ratio e, the cyclic strain history $\boldsymbol{\pi}$ and the shape of the strain loop. In the proposed expression (9) the respective functions describe the following contributions

f_{ampl}:	strain amplitude γ^{ampl}
f_p:	average mean stress p^{av}
f_Y:	average stress ratio $\bar{Y}^{\mathrm{av}}$
f_e:	void ratio e
f_π:	polarization of strain amplitude
$\dot{f}_N^{\,A}, \dot{f}_N^{\,B}$:	number of cycles N

These functions were derived on the basis of the performed cyclic triaxial tests and are presented in the following sections, see also Table 1. The main objective of the cyclic triaxial test program was to separate the above mentioned six parameters, to provide experimental evidence for the assumed dependencies and to determine the material constants.

The irreversible deformation generated by the first so-called *irregular* cycle that is applied next to monotonic loading differs strongly from the accumulation in the subsequent cycles. This accumulation is usually much larger than the accumulation caused by the *regular* (second and subsequent) cycles (Fig. 2), at least for freshly pluviated samples. Therefore this very first cycle must be treated separately. The cycle $N = 1$ refers to the first regular cycle. The irregular cycle and the first regular cycle are calculated implicitly. This is necessary because one needs a representative information about one full regular cycle in order to estimate the strain amplitude, its polarization etc. The irregular cycle is not suitable for this purpose. Note that if the irregular cycle happened to be similar to the subsequent ones (to be actually regular) the above mentioned precaution in the FE calculation is redundant but safe.

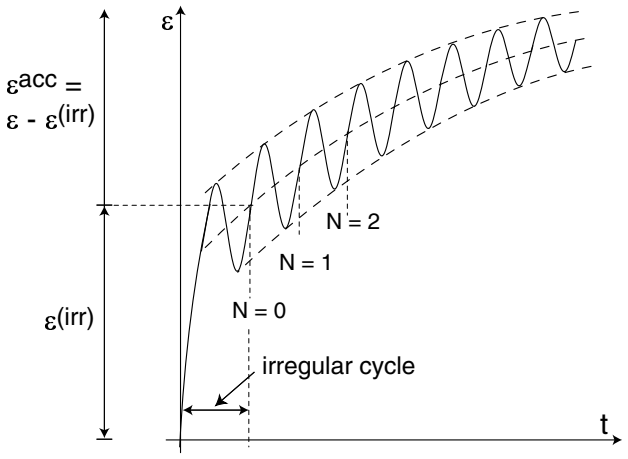

Figure 2. *Irregular* and subsequent *regular* cycles

4 TEST DEVICE AND MATERIAL

A scheme of a typical test device used in the cyclic triaxial tests is presented in Figure 3. The samples were prepared by pluviating dry sand out of a funnel into a cylindrical mould. The samples were either dry or fully saturated. Volume changes were measured via local non-contact displacement transducers or the pore water, respectively. The average and the cyclic vertical force were controlled by a pneumatic loading system. More details on the preparation of samples and the assembly of the test device can be found in Wichtmann et al. (2004a).

All tests were performed on a uniform medium sand (d_{50} = 0.55 mm, U = 1.8). The grain distribution curve, the maximum and minimum void ratios and the critical friction angle are presented in Figure 4.

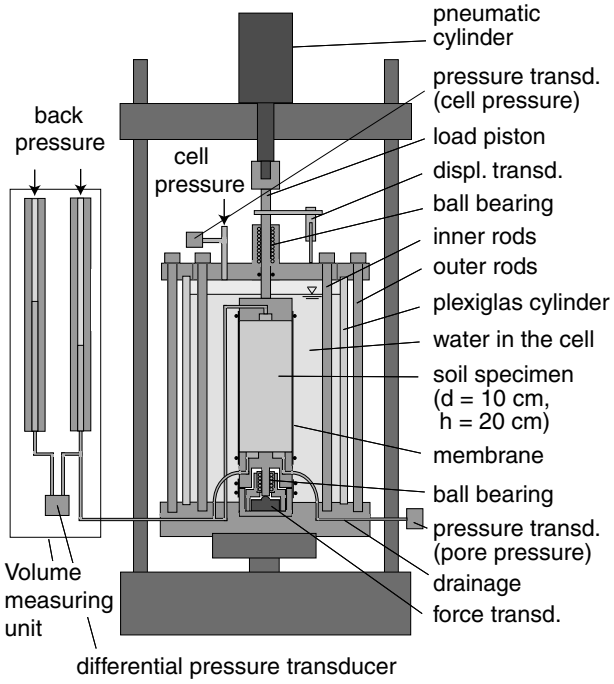

Figure 3. Scheme of cyclic triaxial test device

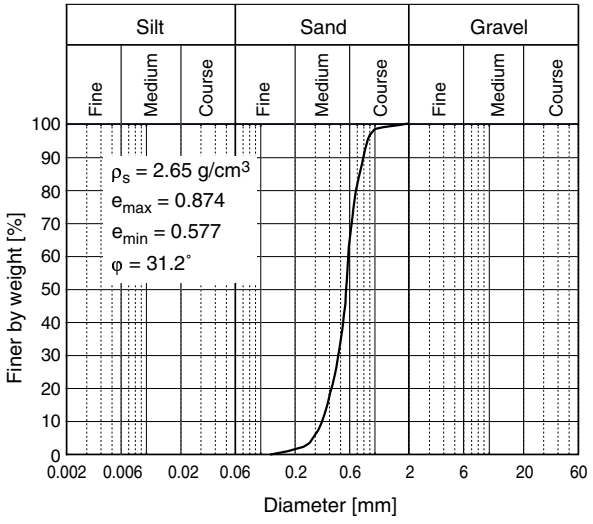

Figure 4. Grain distribution curve, maximum and minimum void ratios and critical friction angle of the used medium sand

5 TEST RESULTS

5.1 *Influence of the strain amplitude*

The strain amplitude is more suitable than the stress amplitude for the description of the accumulation rate because the same strain corresponds approximately to the same mobilized friction angle. As we demonstrate in Section 5.2 the influence of p^{av} cannot be completely eliminated from the model.

The influence of the amplitude on accumulation was studied in a series of tests with varying stress amplitudes between $0.06 \leq \zeta \leq 0.47$ (12 kPa $\leq \sigma_1^{\mathrm{ampl}} \leq$ 94 kPa). The constant average stress was kept at p^{av} = 200 kPa, η^{av} = 0.75 in all tests and the initial relative density of the dry specimens was $0.55 \leq I_{D0} \leq 0.64$, wherein "initial" means after the irregular cycle.

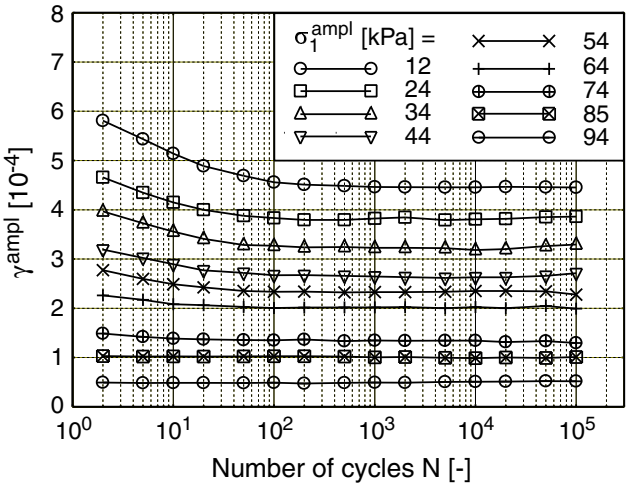

Figure 5. Shear strain amplitude γ^{ampl} as a function of the number of cycles N (all tests: p^{av} = 200 kPa, η^{av} = 0.75, $0.55 \leq I_{D0} \leq 0.64$)

Keeping $\zeta(N)$ constant a small decrease of shear strain amplitude γ^{ampl} with N was noticed, especially during the first 100 cycles and for higher amplitudes (Fig. 6). This variation can be disregarded and $\overline{\gamma} = \int_1^{N_{\max}} \gamma \; \mathrm{d}N/N_{\max}$ is used in the following evaluations.

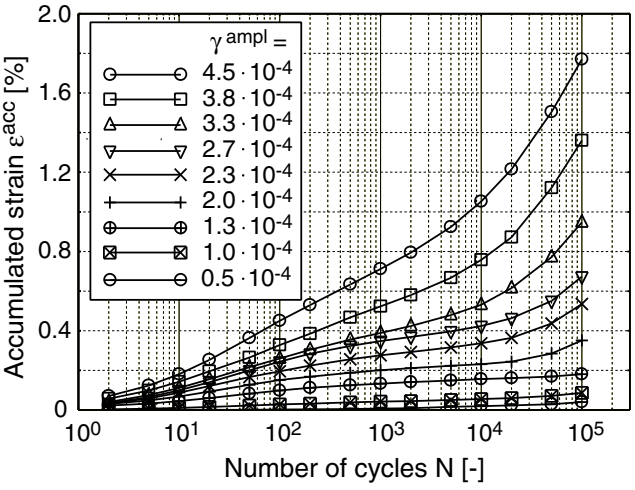

Figure 6. Accumulated strain $\varepsilon^{\mathrm{acc}}$ as a function of the number of cycles N in tests with different shear strain amplitudes γ^{ampl} (all tests: p^{av} = 200 kPa, η^{av} = 0.75, $0.55 \leq I_{D0} \leq 0.64$)

A linear proportionality between ζ and γ^{ampl} was observed. Figure 6 presents the accumulated strain $\varepsilon^{\mathrm{acc}}$ as a function of the number of cycles at different shear strain amplitudes γ^{ampl} in a diagram with semi-logarithmical scale. Only regular cycles are shown. The accumulated strain was found to increase almost linearly with the logarithm of the number of cycles up to $N \approx 1,000$ and then overlogarithmically as discussed in Subsection 5.4. From Figure 6 it can be clearly seen that higher shear strain amplitudes γ^{ampl} cause a larger accumulation $\varepsilon^{\mathrm{acc}}$. In Figure 7 the accumulated strain is presented as a function of the square

of the shear strain amplitude for different numbers of cycles. Accumulation ε^{acc} turns out to increase proportionally to $(\gamma^{\text{ampl}})^2$, independently of N. The following amplitude function

$$f_{\text{ampl}} = \left(\frac{\varepsilon^{\text{ampl}}}{\varepsilon^{\text{ampl}}_{\text{ref}}}\right)^2 = \left(\frac{\gamma^{\text{ampl}}}{\gamma^{\text{ampl}}_{\text{ref}}}\right)^2 \qquad (10)$$

is proposed with the reference amplitude $\gamma^{\text{ampl}}_{\text{ref}} = 10^{-4}$.

On the basis of direct simple shear tests with different shear strain amplitudes Sawicki & Świdziński (1987, 1989) proposed a "common compaction curve", i.e. for identical initial density the curves $\varepsilon^{\text{acc}}(N(\gamma^{\text{ampl}})^2)$ fall together. In Figure 8 the accumulated strain measured in our cyclic triaxial tests is shown as a function of $\tilde{N} = N \cdot (\gamma^{\text{ampl}})^2$. The "common compaction curve" could not be confirmed in our triaxial results.

However, the influence of γ^{ampl} and N cannot be fully uncoupled because the number of cycles as such (irrespectively of their amplitude) is not a good state variable, see discussion in Section 5.4.

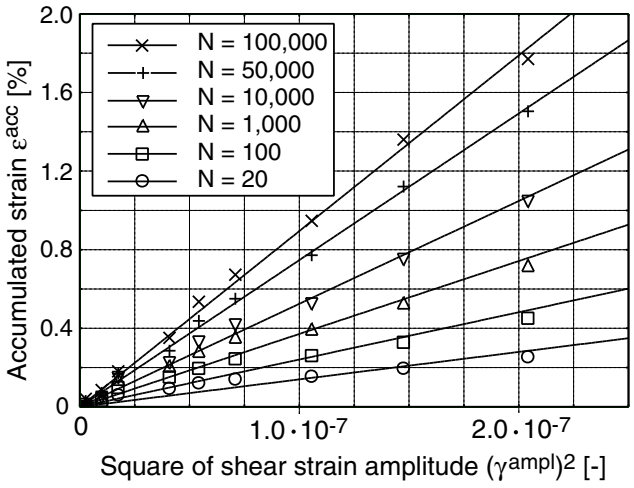

Figure 7. Accumulated strain ε^{acc} as a function of the square of the shear strain amplitude $(\gamma^{\text{ampl}})^2$ for different numbers of cycles N (all tests: p^{av} = 200 kPa, η = 0.75, $0.55 \leq I_{D0} \leq 0.64$)

Figure 9 presents the strain ratio ω as a function of the shear strain amplitude. For higher γ^{ampl} ω was almost independent of γ^{ampl}. At smaller shear strain amplitudes the accumulated volumetric and deviatoric strains were very small and therefore the values of ω could be inaccurate. Thus, the direction of accumulation is assumed to be independent of the shear strain amplitude. Plots of ω over N demonstrate an increase of the volumetric part of the accumulated strain with the number of cycles. This observation was confirmed both with dry and saturated specimens independent on the method of volume measurement.

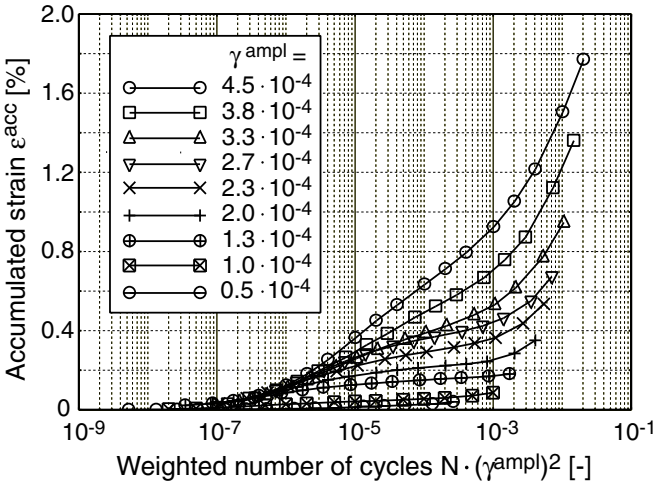

Figure 8. Accumulated strain ε^{acc} in dependence on the weighted number of cycles $\tilde{N} = N \cdot (\gamma^{\text{ampl}})^2$ in tests with different shear strain amplitudes γ^{ampl} (all tests: p^{av} = 200 kPa, η = 0.75, $0.55 \leq I_{D0} \leq 0.64$)

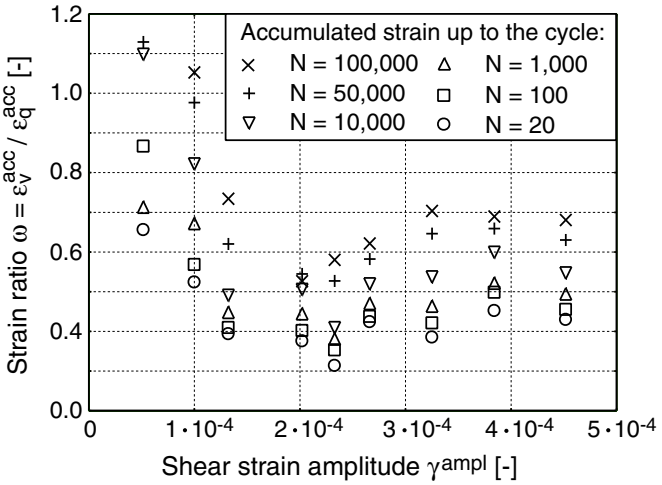

Figure 9. Strain ratio ω as a function of shear strain amplitude γ^{ampl} for different numbers of cycles N (all tests: p^{av} = 200 kPa, η = 0.75, $0.55 \leq I_{D0} \leq 0.64$)

5.2 *Influence of the average stress*

The average stress $\boldsymbol{\sigma}^{\text{av}}$ alone was found to dictate the flow rule **m**. Its influence on the accumulation rate is of crucial importance as demonstrated below.

The average stress $\boldsymbol{\sigma}^{\text{av}}$ was varied between 50 kPa $\leq p^{\text{av}} \leq$ 300 kPa and $-0.88 \leq \eta^{\text{av}} \leq 1.375$. The tests with $\eta^{\text{av}} \geq 0$ (denoted as *cyclic compression tests*) were performed with an amplitude ratio of $\zeta = 0.30$. In the *cyclic extension tests* ($\eta^{\text{av}} \leq 0$) $\zeta = 0.20$, $\zeta = 0.10$ and $\zeta = 0.05$ were used depending on the nearness of $\boldsymbol{\sigma}^{\text{av}}$ to the static failure line. The specimens in both compression and extension tests were prepared within a small range of initial densities ($0.57 \leq I_{D0} \leq 0.69$) and tested under saturated conditions. In the cyclic compression tests 100,000 cycles were applied with a frequency of 1 Hz. For technical reasons, a frequency of 0.1 Hz was used in the cyclic extension tests and the maximum number of cycles was limited to 10,000.

A series of six compression tests with identical average stress ratio (η^{av} = 0.75) but different average mean pressures p^{av} keeping $\zeta = 0.30$ constant (for cyclic stress paths see Fig. 10a) is presented in Figures 11 - 14. The strain amplitudes slightly increased with increasing average mean pressure due to the well known dependence of stiffness $G \sim p^n$ (here: $n = 0.75$), i.e. slightly underproportional to p.

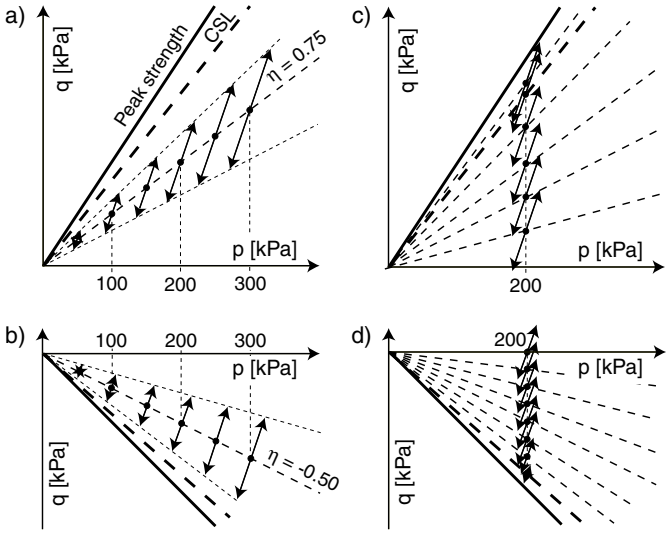

Figure 10. Cyclic stress paths in the tests with different average stresses $\boldsymbol{\sigma}^{av}$

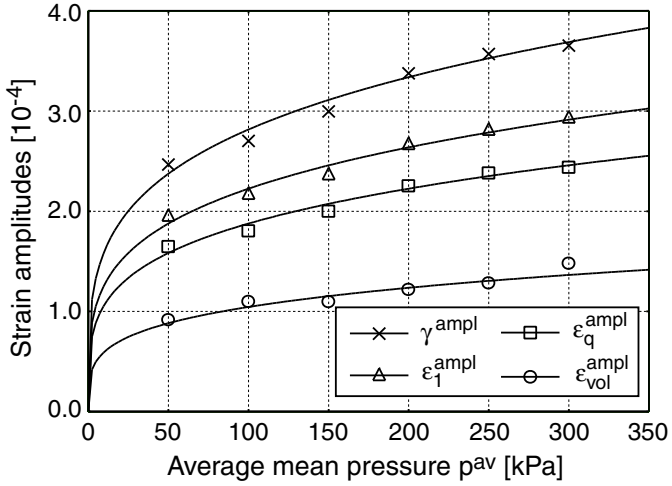

Figure 11. Strain amplitudes in cyclic compression tests with different average mean pressures (all tests: η^{av} = 0.75, ζ = 0.30, $0.61 \leq I_{D0} \leq 0.69$)

Figure 12 presents the accumulated strain as a function of the average mean pressure p^{av} for different numbers of cycles. In this comparison the residual strain has been normalized, i.e. divided by the amplitude function (10). The interesting observation could be made that the accumulated strain significantly *increased* with decreasing average mean pressure. This pressure dependence is stronger for large Ns. The

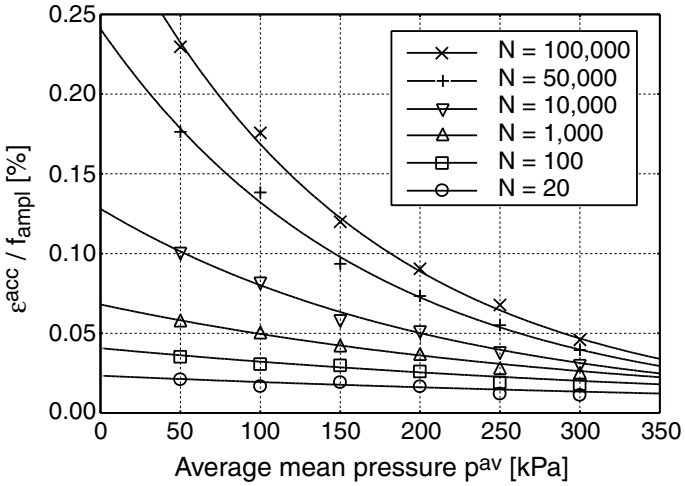

Figure 12. Accumulated strain ε^{acc} divided by the amplitude function f_{ampl} in dependence on the average mean pressure p^{av} for different numbers of cycles (all tests: η^{av} = 0.75, ζ = 0.30, $0.61 \leq I_{D0} \leq 0.69$)

function f_p is proposed in the simple form

$$f_p \;=\; \exp\left[-C_p\left(\frac{p^{av}}{p_{atm}} - 1\right)\right]. \qquad (11)$$

The atmospheric pressure p_{atm} = 100 kPa is used as a reference for which $f_p = 1$ holds. Equation (11) was fitted to the data in Figure 12 for different numbers of cycles. The corresponding curves are shown as solid lines in Figure 12. Actually the parameter C_p could be made dependent on the number of cycles, however, in order to keep the number of material constants manageable, a constant value of C_p is proposed. In accordance with remarks later in this subsection the material constant was chosen to be $C_p = 0.44$.

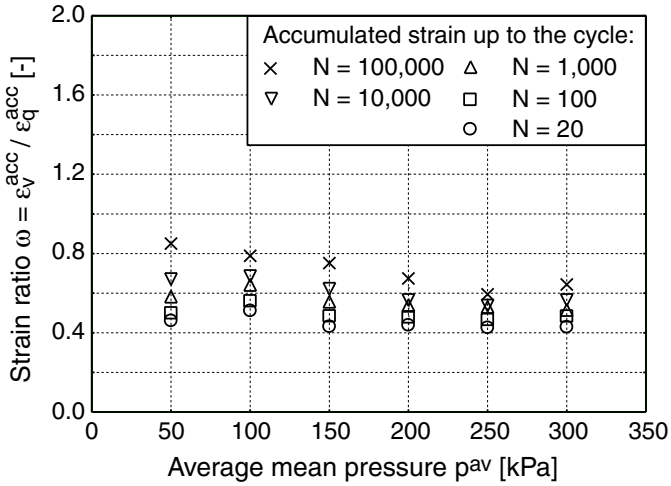

Figure 13. Strain ratio ω as a function of average mean pressure p^{av} for different numbers of cycles N (all tests: η^{av} = 0.75, ζ = 0.30, $0.61 \leq I_{D0} \leq 0.69$)

The direction of accumulation was found to be relatively unsensitive to changes in the average mean pressure keeping η^{av} constant (Fig. 13). However, a

slight increase of strain ratio ω with decreasing average mean pressure could be observed. Moreover a slight increase of ω with N could be monitored. Of course, having reached a theoretical state of maximum density this tendency is expected to inverse, i.e. only deviatoric accumulation will be possible.

Six cyclic extension tests varying the average mean pressure (50 kPa $\leq p^{av} \leq$ 300 kPa) but holding η^{av} = -0.5 constant were performed. The amplitude ratio was ζ = 0.20 and all initial densities I_{D0} lay between 0.62 and 0.66. The cyclic stress paths are presented in Fig. 10b.

In Figure 14 the measured strain amplitudes are plotted versus p^{av}. A proportionality $G \sim p^n$ was observed but the exponent was found to be n = 0.52, which is close to values determined from dynamic tests on the respective sand (Wichtmann & Triantafyllidis 2004a,b) and less than the value measured in the cyclic compression tests (probably due to higher amplitudes in the latter case).

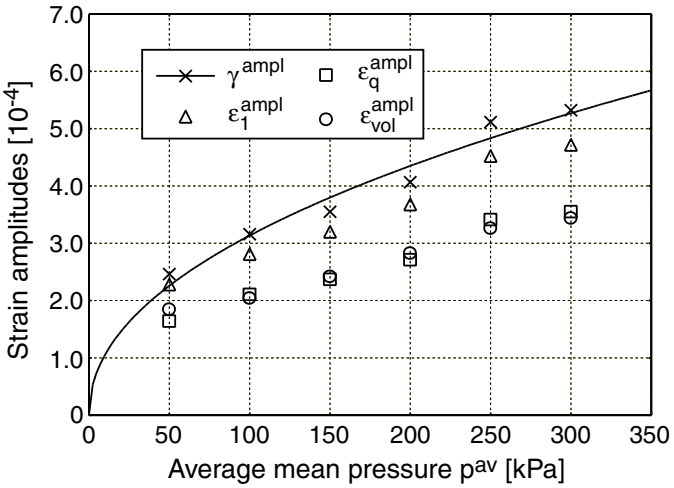

Figure 14. Strain amplitudes in cyclic extension tests with different average mean pressures (all tests: η^{av} = -0.50, ζ = 0.20, $0.62 \leq I_{D0} \leq 0.66$)

Figure 15 presents the accumulated strain normalized by f_{ampl} as a function of the average mean pressure. As in the cyclic compression tests accumulation increased with decreasing p^{av}. The function f_p also fits well these test results for $p^{av} \geq 100$ kPa. However, the large accumulation in the test with p^{av} = 50 kPa is not captured by f_p. Fitting f_p to the tests with $p^{av} \geq 100$ kPa lead to material constants that increased from C_p = 0.08 for N = 20 to C_p = 0.44 at N = 10,000 (comparable to the cyclic compression tests). Also for $\eta^{av} \leq 0$ the direction of accumulation was found to be independent of p^{av} for η^{av} = const. (Fig. 16).

The dependence $\varepsilon^{acc}(N)$ observed in both average compression and extension tests of these series is in agreement with the shape of the curves shown in Figure 6.

The results of a series of eleven tests with $0.375 \leq \eta^{av} \leq 1.375$ ($0.088 \leq \bar{Y}^{av} \leq 1.243$) and p^{av} = 200 kPa = const and ζ = const (for cyclic stress paths see Fig. 10c) are presented in Figures 17 - 19.

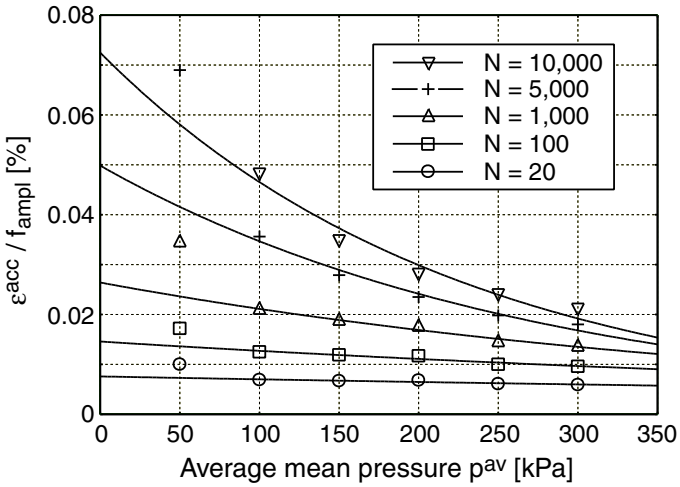

Figure 15. Accumulated strain ε^{acc} divided by the amplitude function f_{ampl} in dependence on the average mean pressure p^{av} for different numbers of cycles (all tests: η^{av} = -0.50, ζ = 0.20, $0.62 \leq I_{D0} \leq 0.66$)

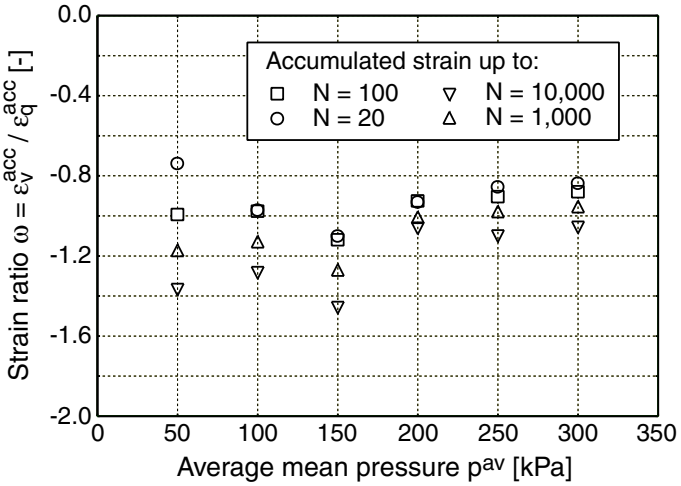

Figure 16. Strain ratio ω as a function of average mean pressure p^{av} for different numbers of cycles N (all tests: η^{av} = -0.50, ζ = 0.20, $0.62 \leq I_{D0} \leq 0.66$)

The strain amplitudes slightly decreased with increasing η^{av} as shown in Figure 17. The accumulated strain for normalized amplitude over stress ratio $\bar{Y}^{av}$ is plotted for different numbers of cycles in Figure 18. The accumulation increases with $\bar{Y}^{av}$. For $\bar{Y}^{av} >$ 1.243 ($\eta >$ 1.375) the rate of accumulation suddenly explodes reaching nearly 20 % after 100,000 cycles. This can be explained by the fact that for $\bar{Y}^{av}$ = 1.243 the maximum deviatoric stress $q^{max} = q^{av} + q^{ampl}$ during a load cycle lies above the peak friction angle $\varphi_p = 36.8°$ obtained for $I_D = 0.63$ in static triaxial tests. Below this limit the function f_Y can be fairly well approximated by

$$f_Y = \exp\left(C_Y \, \bar{Y}^{av}\right) \qquad (12)$$

The material constant $1.77 \leq C_Y \leq 2.25$ can be shown to be rather independent of the number of cy-

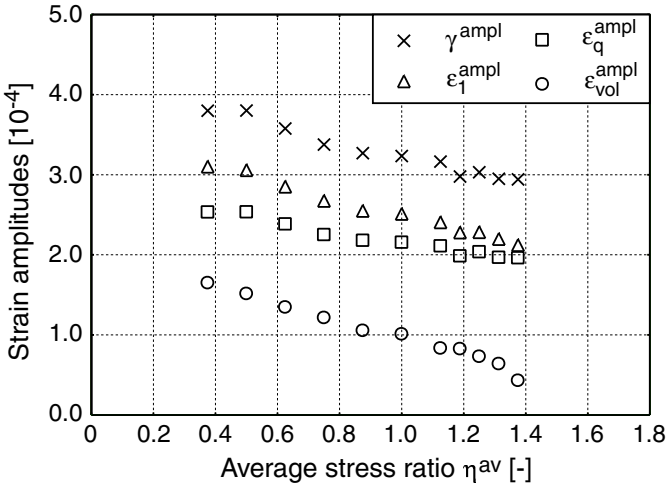

Figure 17. Strain amplitudes in tests with different average stress ratios $\eta^{\text{av}} \geq 0$ (all tests: p^{av} = 200 kPa, ζ = 0.30, $0.57 \leq I_{D0} \leq 0.67$)

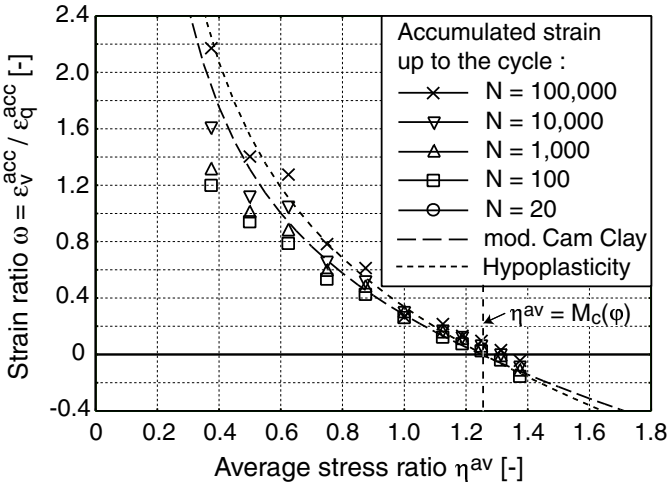

Figure 19. Strain ratio ω as a function of average stress ratio $\eta^{\text{av}} \geq 0$ for different numbers of cycles N (all tests: p^{av} = 200 kPa, ζ = 0.30, $0.57 \leq I_{D0} \leq 0.67$)

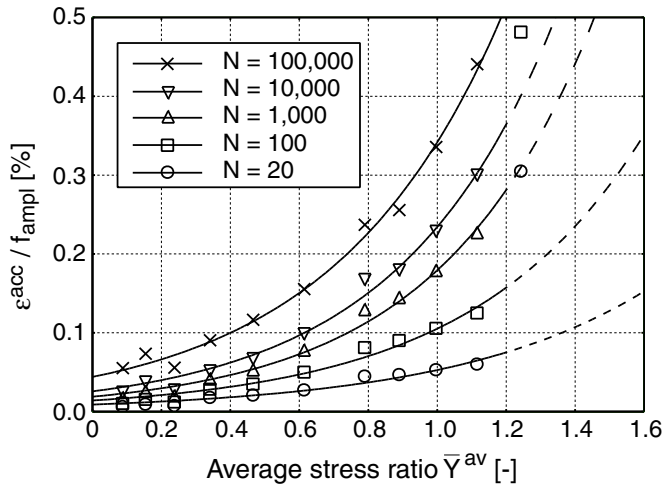

Figure 18. Accumulated strain ε^{acc} divided by the amplitude function f_{ampl} in dependence on the average stress ratio $\bar{Y}^{\text{av}}$ for different numbers of cycles (all tests: p^{av} = 200 kPa, ζ = 0.30, $0.57 \leq I_{D0} \leq 0.67$)

cles. The value C_Y = 2.05 for N = 100,000 is set into approach in the material model. For isotropic ($\bar{Y}^{\text{av}} = 0$) stresses $f_Y = 1$ holds.

Figure 19 shows the measured values of strain ratio ω plotted over η^{av}. A decrease of ω with η^{av} is evident, i.e. with increasing deviatoric part of the average state of stress the accumulation gets more deviatoric, too. The critical stress ratio $M_c(\varphi)$ was determined from static tests. For $\eta^{\text{av}} < M_c(\varphi)$ densification was observed. Specimens with an average stress above the critical state line exhibited a dilative behavior. This is in accordance with experimental results of Luong (1982) and Chang & Whitman (1988). Especially for large numbers of cycles ($N = 100,000$) the dependence $\omega(\eta^{\text{av}})$ conforms with the flow rule of the modified Cam Clay model $\omega = ({M_c}^2 - \eta^2)/(2\eta)$ as already suggested by Chang & Whitman (1988). The agreement with the hypoplastic theory (K-model, see Niemunis 2003) is also satisfactory. In our constitutive model we ignore the change of the direction of accumulation with the number of cycles. The hypoplastic flow rule is used for **m**.

Six tests with average extension were performed with stress ratios varying in the range $-0.88 \leq \eta^{\text{av}} \leq 0$ and with a constant average mean pressure p^{av} = 200 kPa. The samples were prepared with similar initial densities $0.60 \leq I_{D0} \leq 0.66$. Amplitude ratios of ζ = 0.20 were used in the tests with $-0.625 \leq \eta^{\text{av}} \leq 0$. For higher amounts of the stress ratios η^{av} the amplitude ratio was reduced in order to keep the minimum deviatoric stress $q^{\min} = q^{\text{av}} - q^{\text{ampl}}$ above the static failure line. Therefore, at η^{av} = -0.75 and η^{av} = -0.88 the amplitude ratios ζ = 0.10 and ζ = 0.05 were used, respectively. The corresponding cyclic stress paths are shown in Figure 10d.

Figure 20 presents the strain amplitudes measured in the tests with ζ = 0.20. With increasing stress ratio η^{av} (i.e. with decreasing absolute value) the amplitudes decreased. Similar conclusions could be drawn from Figure 17.

Figure 21 shows the accumulated strain normalized with f_{ampl} as a function of the stress ratio $\bar{Y}^{\text{av}}$ (positive also in the extension case). Approaching the failure line the intensity of accumulation accelerated. In the test with η^{av} = -0.88 ($\bar{Y}^{\text{av}}$ = 0.989) the accumulation rate rapidly grew leading to $\varepsilon^{\text{acc}}/f_{\text{ampl}}$ = 0.29 after 10,000 cycles. This is due to the minimum deviatoric stress $q_{\min}$ being very close to the static failure line. The data of this test is not included in Figure 21 and is not captured by the proposed formulas. Similar observations were made in the cyclic compression tests for η^{av} = 1.375 with $q^{\max}$ lying above the failure line. The function f_Y of Equation (12) could be fitted well to the experimental data in Figure 21 resulting in material constants $2.17 \leq C_Y \leq 3.14$ for different numbers of cycles. For N = 10,000 $C_Y = 2.17$ was determined lying close to C_Y = 2.15 obtained for N

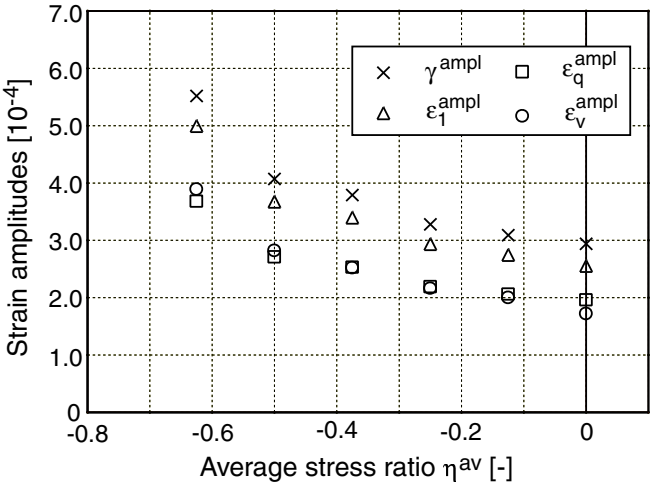

Figure 20. Strain amplitudes in tests with different stress ratios ($\eta^{av} \leq 0$) (all tests: p^{av} = 200 kPa, ζ = 0.20, $0.60 \leq I_{D0} \leq 0.66$)

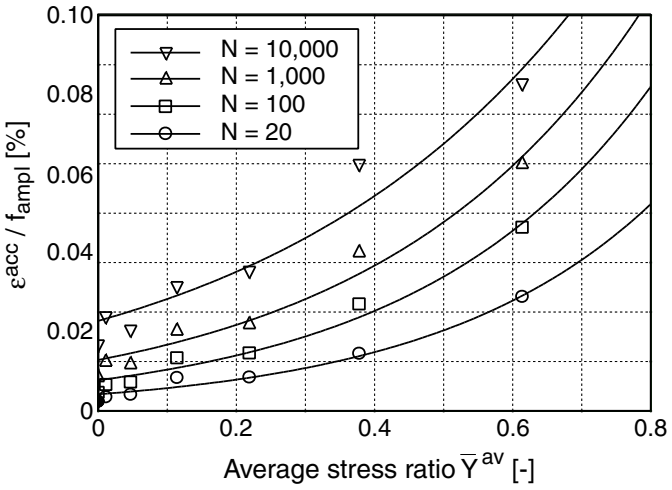

Figure 21. Accumulated strain divided by the amplitude function f_{ampl} in dependence on the average stress ratio $\bar{Y}^{av}$ (all tests: p^{av} = 200 kPa, $0.60 \leq I_{D0} \leq 0.66$)

= 100,000 from the cyclic compression tests. Thus, it can be concluded that the function f_Y proposed for compression can be used for $\boldsymbol{\sigma}^{av}$ in triaxial extension keeping C_Y = 2.15.

Figure 22 presents the measured ω for extension and compares them with two theoretical flow rules for monotonic loading. With increasing absolute value of η^{av} the accumulation becomes more deviatoric. At an average stress lying on the critical state line the accumulation was pure deviatoric. As observed in the cyclic compression tests the volumetric portion of the accumulation increased with the number of cycles, especially for small values of η^{av}. The hypoplastic flow rule fits better the observed material behavior than the modified Cam-clay model.

Next tests with average mean pressures p^{av} = 100 kPa and p^{av} = 300 kPa and different stress ratios $\eta^{av} > 0$ (ζ = 0.30 = const.) were performed in order to study if the functions f_p and f_Y can be treated separately or if a more complex description $\dot{\varepsilon}^{acc}(\boldsymbol{\sigma}^{av})$ via

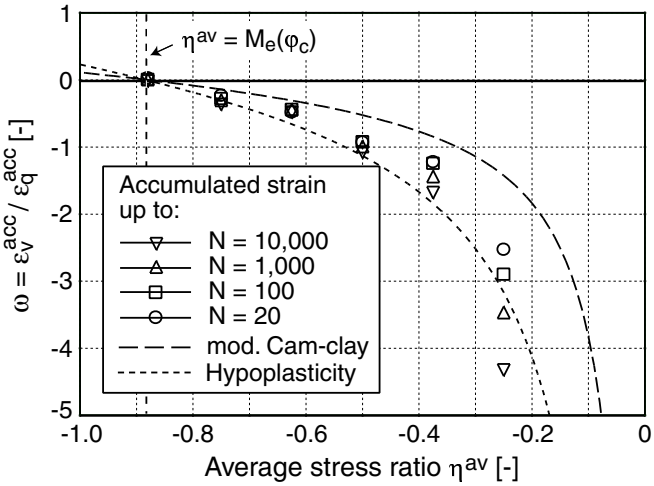

Figure 22. Strain ratio ω as a function of the average stress ratio η^{av} for different numbers of cycles N (all tests: p^{av} = 200 kPa, $0.60 \leq I_{D0} \leq 0.66$)

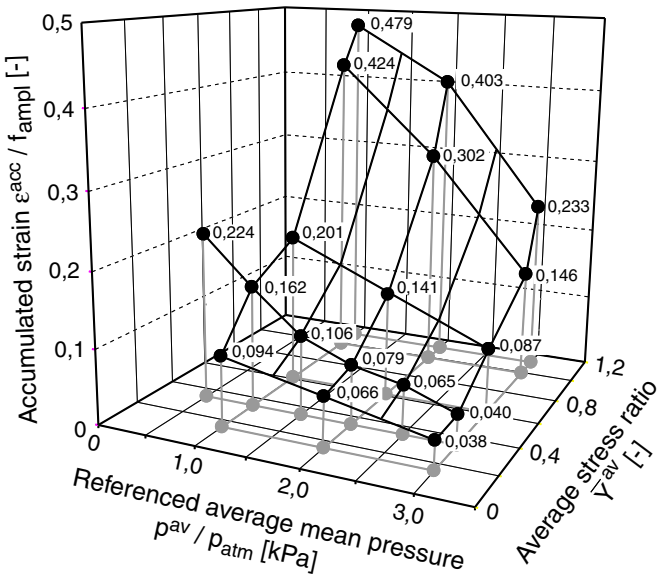

Figure 23. Accumulated strains ε^{acc} after 100,000 load cycles for different average stresses (all tests: ζ = 0.30, $0.57 \leq I_{D0} \leq 0.69$)

$f(p^{av}, \bar{Y}^{av})$ is needed.

In Figure 23 the residual strain is presented after 100,000 cycles as a function of the normalized average mean pressure p^{av}/p_{atm} and the average stress ratio $\bar{Y}^{av}$. Figure 23 confirms, that everywhere the accumulation increases with *decreasing* average mean pressure p^{av} and increasing deviatoric stress $\bar{Y}^{av}$.

Figure 24 shows, that the parameter C_p of the function f_p after N = 100,000 cycles is (despite some amount of scattering) relatively independent of the stress ratio η^{av}. A dependence of C_p on the number of cycles was found also in these tests. However, the influence of the number of cycles on C_p is less pronounced for high stress ratios $\eta^{av} \geq 1.25$. In our material model the mean value of C_p = 0.44 after 100,000 cycles is set into approach.

The function f_Y determined from tests with p^{av} =

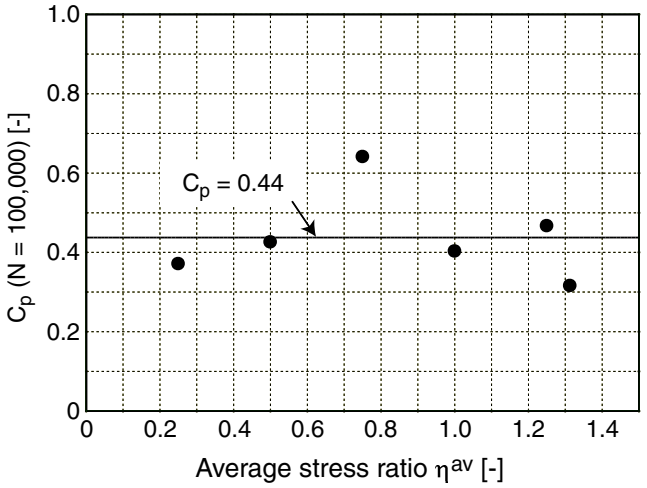

Figure 24. Parameter C_p of function f_p for N = 100,000 and different stress ratios η^{av}

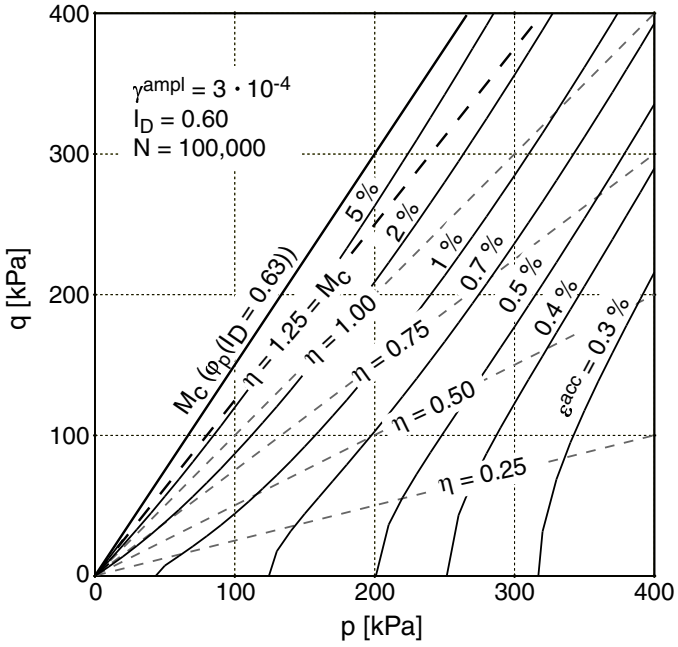

Figure 25. Curves of identical accumulation in the p - q - plane

200 kPa could be confirmed in the tests with p^{av} = 100 kPa and p^{av} = 300 kPa. In the case of the smaller pressure values between 1.64 and 2.32 were obtained for C_Y and different numbers of cycles, at the higher pressure $1.61 \leq C_Y \leq 2.26$ was determined (for comparison: $1.77 \leq C_Y \leq 2.25$ for p^{av} = 200 kPa). Thus, the use of $C_Y = 2.05$ for $p^{av} \neq 200$ kPa seems justified.

We conclude that f_p and f_Y as uncoupled functions can be admitted. Figure 25 presents curves of identical accumulation for $N = 100,000$, $\gamma^{ampl} = 3 \cdot 10^{-4}$, I_{D0} = 0.60. In a wide range of the p - q - plane the curves ε^{acc} = const. run almost parallel to the line of maximum shear strength $\eta = M_c(\varphi_p)$.

The direction of accumulation at different average stresses $\boldsymbol{\sigma}^{av}$ is shown in Figure 26. The direction of accumulation is expressed by a unit vector with starting point at (p^{av}, q^{av}). Only few of the large amount of performed tests are shown in the case of p^{av} = 200 kPa and $\eta^{av} \geq 0$.

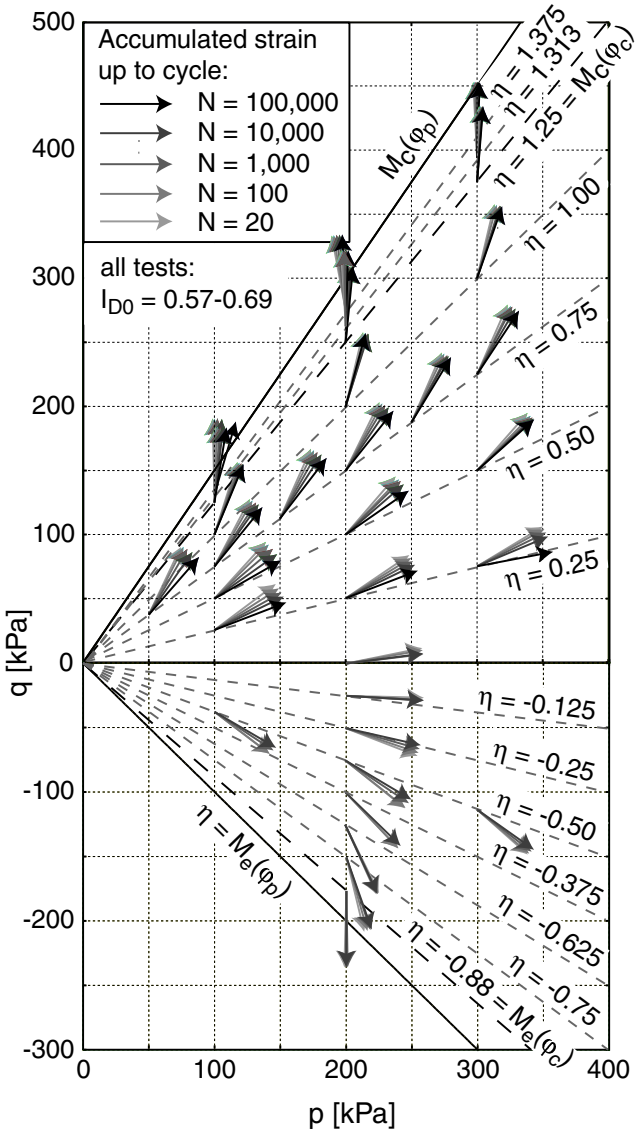

Figure 26. Direction of accumulation in the p - q - plane for different average stresses (all tests: ζ = 0.30, $0.57 \leq I_{D0} \leq 0.69$)

5.3 *Influence of the void ratio*

Different initial void ratios ($0.580 \leq e_0 \leq 0.688$, $0.63 \leq I_{D0} \leq 0.99$) were tested. The average stress (p^{av} = 200 kPa, η^{av} = 0.75) and the amplitude ratio (ζ = 0.30) were held constant within this series. The specimens were water-saturated.

Figure 27 presents the strain amplitudes as a function of the initial void ratio e_0. The condition ζ = const. implies slightly higher strain amplitudes for lower initial densities, because the shear modulus G decreases with void ratio e. Fitting

$$G(e) \sim \frac{(a-e)^2}{1+e} \qquad (13)$$

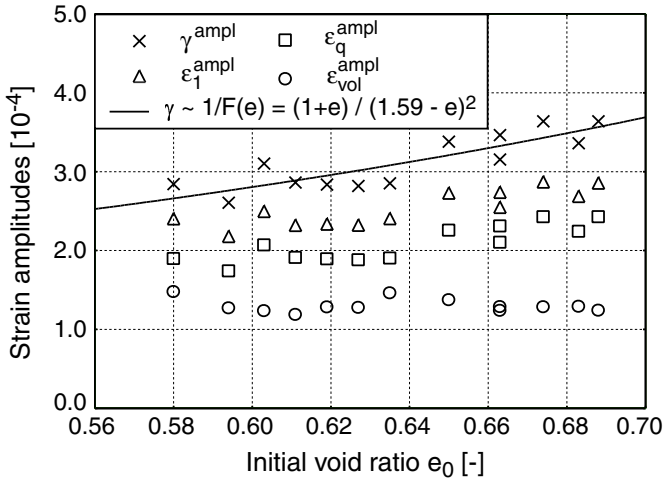

Figure 27. Strain amplitudes in tests with different initial void ratios e_0 (all tests: p^{av} = 200 kPa, η^{av} = 0.75, ζ = 0.30)

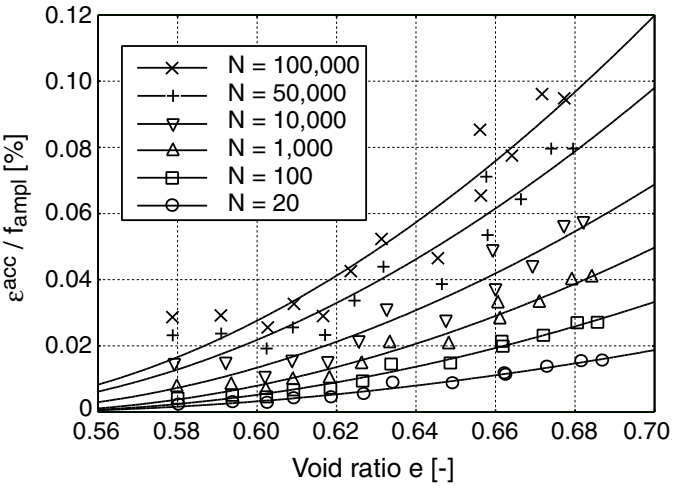

Figure 28. Accumulated strain ε^{acc} divided by the amplitude function f_{ampl} in dependence on the actual void ratio e for different numbers of cycles (all tests: p^{av} = 200 kPa, η^{av} = 0.75, ζ = 0.30)

of Hardin & Black (1966) to the curve of shear strain amplitude over void ratio ($\gamma \sim 1/G(e)$) leads to a = 1.59. In dynamic tests on the same sand (tests in a resonant column device and comparative tests measuring wave velocities with piezoelectric elements in a triaxial cell, Wichtmann & Triantafyllidis 2004a,b) a = 1.46 was determined for amplitudes $\gamma^{\text{ampl}} \approx 10^{-6}$. Thus, a quite similar relationship $\gamma^{\text{ampl}}(e)$ was found.

As it can be seen from Figure 28 the rate of accumulation is high for loose soils. The accumulated strains in Figure 28 are normalized with the amplitude function (10). Therefore the increase of the accumulation rate with increasing void ratio in Figure 28 cannot be attributed to the increase of shear strain amplitude with void ratio. The following function (similar to (13)) was found to describe the cyclic void ratio dependence:

$$f_e = \frac{(C_e - e)^2}{1+e} \frac{1+e_{\text{ref}}}{(C_e - e_{\text{ref}})^2} \qquad (14)$$

The material constant $C_e = 0.52$ was found to be independent of the number of cycles. The reference void ratio is $e_{\text{ref}} = e_{\max} = 0.874$, i.e. $f_e = 1$ holds true for $e = e_{\max}$. The data in Figure 28 has a larger scatter than in the presentations of the cyclic triaxial tests with variation of stress amplitude and average state of stress, respectively. We contribute this to the method of sample preparation since different outlet diameters of the funnel were used.

In Figure 29a curves of identical accumulation ε^{acc} = const. are plotted in the semi-logarithmically scaled p - e - plane for N = 100,000, $\gamma^{\text{ampl}} = 3 \cdot 10^{-4}$ and I_{D0} = 0.60. From the schemes in Figure 29b it is obvious that the inclination of the curves of identical accumulation ε^{acc} = const. is opposite to the curves of identical material behaviour under monotonic shearing. Thus, the concept of critical void ratio is not appropriate for cyclic loading. For this reason the usage of a coupled function $f(e, p^{\text{av}})$ seems inconvenient.

The direction of accumulation was found to be independent of the void ratio for the range of densities presented in Figure 30. For $I_{D0} > 0.90$ discrepancies in the strain ratios ω were large and therefore these strain ratios have been excluded from Figure 30. The scatter can be attributed to ω calculated as a quotient of two very small quantities.

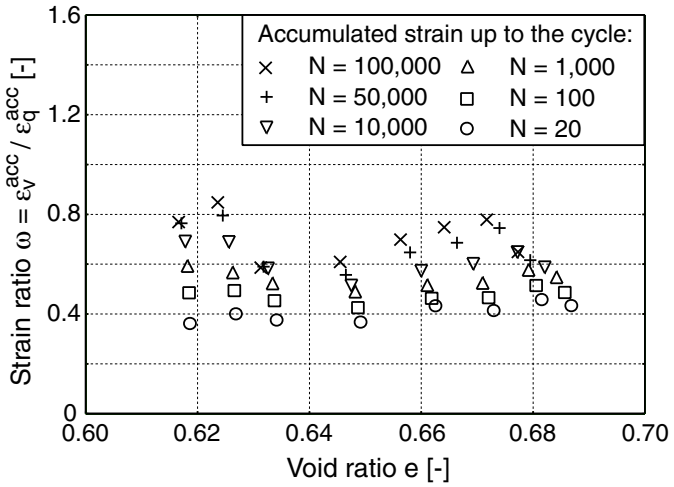

Figure 30. Strain ratio ω as a function of actual void ratio e for different numbers of cycles N (all tests: p^{av} = 200 kPa, η^{av} = 0.75, ζ = 0.30)

5.4 *Influence of the number of cycles*

As already mentioned the accumulated strain grows faster than the logarithm of the number of cycles, especially for large numbers of cycles N. For a constant strain amplitude $\varepsilon^{\text{acc}}(N)$ could therefore be proposed to consist of a logarithmic and a linear part

$$\varepsilon^{\text{acc}}(N) \sim C_{N1}\left[\ln\left(1 + C_{N2}N\right) + C_{N3}N\right]$$
$$= \underbrace{C_{N1}\ln\left(1 + C_{N2}N\right)}_{\varepsilon^{\text{acc}\ A}} + \underbrace{C_{N1}C_{N3}N}_{\varepsilon^{\text{acc}\ B}} \qquad (15)$$

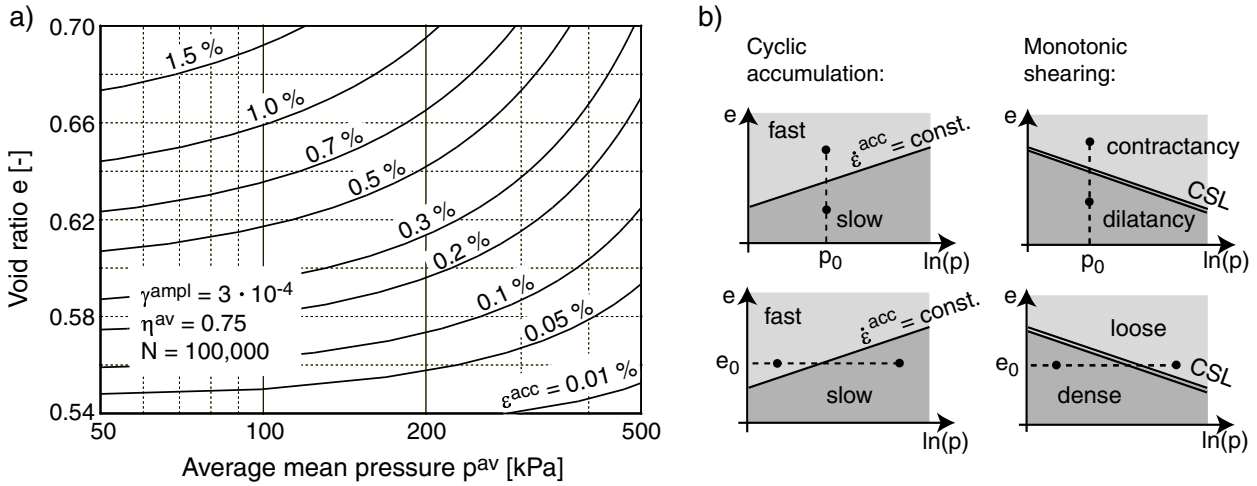

Figure 29. *a) Curves of identical accumulation in the p - e - diagram, b) Comparison with the concept of critical void ratio*

Introducing the accumulated structural strain $\varepsilon^{\text{acc }A}$ as a state variable one may write the rates as

$$\begin{aligned} \dot{f}_N^{\,A} &= C_{N1} C_{N2} \exp\left(-\frac{\varepsilon^{\text{acc }A}}{f_i\, C_{N1}}\right) \\ \dot{f}_N^{\,B} &= C_{N1} C_{N3} \end{aligned} \tag{16}$$

with the abbreviation $f_i = f_{\text{ampl}}\ f_p\ f_Y\ f_e\ f_\pi$. As demonstrated by Niemunis et al. (2004) using $\varepsilon^{\text{acc }A}$ as a state variable (i.e. the combined effect of N and $\varepsilon^{\text{ampl}}$ rather than N) enables the material model to capture packages of cycles with varying amplitudes.

In order to determine the material constants C_{Ni} the accumulation $\varepsilon^{\text{acc}}(N)$ measured in the cyclic triaxial tests is divided by the functions f_{ampl}, f_p, f_Y, f_e and f_π and represented as a function of N in Figure 31. In the cyclic triaxial case $f_\pi = 1$ holds true since the polarization of the strain amplitude is not changed during cyclic loading. Figure 31 does not contain the test with the maximum deviatoric stress $q^{\max} > M_c(\varphi_p)$ because it lies beyond the scope of our formulas. Also the tests with $I_{D0} > 0.90$ are excluded from fitting of the function f_N because of the scatter of data. All other curves lie within a narrow band. The curve presented as solid line in Figure 31 corresponds to Equation (15) with $C_{N1} = 1.9 \cdot 10^{-4}$, $C_{N2} = 0.547$ and $C_{N3} = 5.78 \cdot 10^{-5}$. Equation (15) alone describes $\varepsilon^{\text{acc}}(N)$ for $\gamma^{\text{ampl}} = \gamma_{\text{ref}}^{\text{ampl}}$, $p^{\text{av}} = p_{\text{atm}}$, $\bar{Y}^{\text{av}} = 0$ and $e = e_{\max}$, i.e. for all other functions equal 1.

In three additional tests 2,000,000 cycles with a frequency of 1 Hz were applied to saturated specimens at an average stress p^{av} = 200 kPa, η^{av} = 0.75. An amplitude ratio of ζ = 0.30 was used. Figure 32 shows the development of the residual strain ε^{acc} normalized by the amplitude function f_{ampl} with the number of cycles. It becomes clear that in the semi-logarithmic diagram even after 2,000,000 cycles no abation of the accumulation could be detected and the curves still

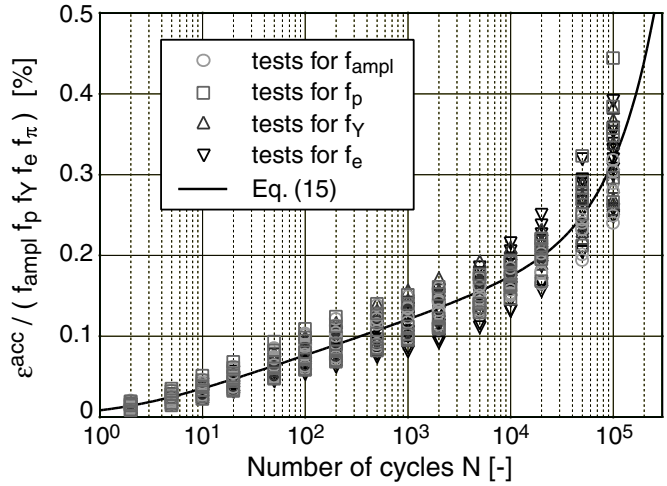

Figure 31. Accumulated strain ε^{acc} divided by the functions f_{ampl}, f_p, f_Y, f_e and f_π as a function of the number of cycles

grow faster than the logarithm of N. Thus, Equation (15) is also valid for $N > 100,000$.

However, some lack of clarity exists concerning the evaluation of the direction of accumulation with N at higher numbers of cycles. In two of the three tests (Nos. 1 and 3, performed in different triaxial devices) a huge increase of ω especially after 500,000 cycles was measured (Fig. 33) while in the third test this increase was much less. It is not clear up to now, if these observations are caused by real material behaviour or if they are due to errors in the testing procedure (e.g. diffusion processes of cell water through the membrane into the specimen over the long duration of a test (approximately 4 weeks)). Further experimental work is planned on this field.

6 SUMMARY AND CONCLUSIONS

Numerous cyclic triaxial tests with varying average stresses (triaxial compression and extension), amplitudes and initial densities were performed. The main conclusions from these tests are:

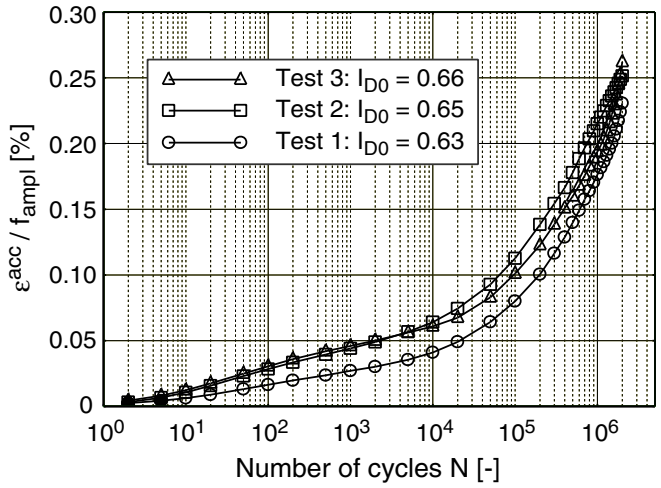

Figure 32. Accumulated strain ε^{acc} divided by the amplitude function f_{ampl} as a function of the number of cycles in tests with $N_{\max} = 2 \cdot 10^6$ cycles (all tests: p^{av} = 200 kPa, η^{av} = 0.75, ζ = 0.30)

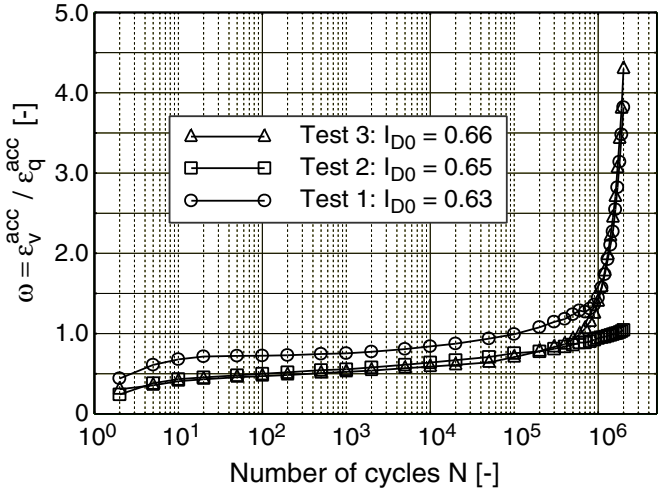

Figure 33. Strain ratio ω plotted against the number of cycles N in tests with $N_{\max} = 2 \cdot 10^6$ cycles (all tests: p^{av} = 200 kPa, η^{av} = 0.75, ζ = 0.30)

- The residual strain ε^{acc} increases with the number of cycles while the accumulation rate $\dot{\varepsilon}^{\text{acc}}$ decreases.
- The accumulated strain ε^{acc} increases faster than the logarithm of the number of cycles N.
- The accumulation rate does not vanish even after an application of $2 \cdot 10^6$ cycles.
- The strain accumulation is proportional to the square of the shear strain amplitude, $\varepsilon^{\text{acc}} \sim (\gamma^{\text{ampl}})^2$.
- The so-called "common compaction curve" (Sawicki & Świdziński 1987, 1989) could not be reproduced in the triaxial tests.
- The direction of accumulation does not depend on the applied shear strain amplitude.
- The volumetric part of the direction of accumulation slightly increases with the number of cycles.

Function	Mat. constants	
$f_{\text{ampl}} = \left(\dfrac{\gamma^{\text{ampl}}}{\gamma^{\text{ampl}}_{\text{ref}}} \right)^2$	$\gamma^{\text{ampl}}_{\text{ref}}$	10^{-4}
$\dot{f}_N^A = C_{N1} C_{N2} \exp\left(-\dfrac{\varepsilon^{\text{acc}\ A}}{f_i\ C_{N1}} \right)$	C_{N1}	$1.9 \cdot 10^{-4}$
$\dot{f}_N^B = C_{N1} C_{N3}$	C_{N2}	0.547
	C_{N3}	$5.78 \cdot 10^{-5}$
$f_p = \exp\left[-C_p \left(\dfrac{p^{\text{av}}}{p_{\text{atm}}} - 1 \right) \right]$	C_p	0.44
	p_{atm}	100 kPa
$f_Y = \exp\left(C_Y\ \bar{Y}^{\text{av}} \right)$	C_Y	2.05
$f_e = \dfrac{(C_e - e)^2}{1+e} \dfrac{1 + e_{\text{ref}}}{(C_e - e_{\text{ref}})^2}$	C_e	0.520
	e_{ref}	0.874
$f_\pi = 1 + C_{\pi 1} \left[1 - \left(\overrightarrow{\mathbf{A}}_\varepsilon :: \boldsymbol{\pi} \right)^{C_{\pi 2}} \right]$	$C_{\pi 1}$	4.0
$\dot{\boldsymbol{\pi}} = C_{\pi 3} \left(\overrightarrow{\mathbf{A}}_\varepsilon - \boldsymbol{\pi} \right) \ \|\mathbf{A}_\varepsilon\|^2$	$C_{\pi 2}$	0.5
	$C_{\pi 3}$	178.4

Table 1. Summary of the partial functions f_i and a list of the material constants C_i for the tested sand

- The accumulated strain ε^{acc} increases with decreasing average mean pressure p^{av} for $\boldsymbol{\sigma}^{\text{av}}$ in both cases $\eta^{\text{av}} \leq 0$ and $\eta^{\text{av}} \geq 0$.
- The dependence of the direction of accumulation on the average mean pressure p^{av} is negligible.
- The accumulated strain ε^{acc} increases with increasing average stress ratio $\bar{Y}^{\text{av}}$, i.e. with an approach toward the failure lines (valid for $\boldsymbol{\sigma}^{\text{av}}$ in compression and extension).
- If the maximum or minimum deviatoric stress during a cycle $q^{\max} = q^{\text{av}} + q^{\text{ampl}}$ or $q^{\min} = q^{\text{av}} - q^{\text{ampl}}$ approaches or exceeds the static failure lines the rate of accumulation rapidly increases.
- The direction of accumulation is in agreement with the flow rules of the modified Cam-clay model and the hypoplastic K-model for $\eta^{\text{av}} \geq 0$. For $\eta^{\text{av}} \leq 0$ the hypoplastic flow rule fits better the observed material behaviour.
- The accumulated strain ε^{acc} is greater for looser material, see f_e.
- The direction of accumulation does not significantly depend on the void ratio, at least for the tested range of densities.

An explicit material model was proposed on the basis of the cyclic triaxial test results in conjunction with experimental findings concerning the influence of the shape and the polarization of the strain loop presented in the companion paper, Wichtmann et al. (2004b). Table 1 summarizes the functions f_i and the material constants C_i of the proposed model.

7 ACKNOWLEDGEMENTS

The authors are grateful to DFG (German Research Council) for the financial support. This study is a part of the project A8 "Influence of the fabric changes in soil on the lifetime of structures" of SFB 398 "Lifetime oriented design concepts".

REFERENCES

Bouckovalas, G., Whitman, R.V. & Marr, W.A. 1984. Permanent displacement of sand with cyclic loading. *Journal of Geotechnical Engineering* 110(11): 1606-1623.

Chang, C.S. & Whitman, R.V. 1988. Drained permanent deformation of sand due to cyclic loading. *Journal of Geotechnical Engineering* 114(10): 1164-1180.

Ko, H.Y. & Scott, R.F. 1967. Deformation of sand in hydrostatic compression. *Journal of the Soil Mechanics and Foundations Division* 93(SM3): 137-156.

Luong, M.P. 1982. Mechanical aspects and thermal effects of cohesionless soils under cyclic and transient loading. In *Proc. IUTAM Conf. on Deformation and Failure of Granular Materials, Delft*: 239-246.

Marr, W.A. & Christian, J.T. 1981. Permanent displacements due to cyclic wave loading. *Journal of the Geotechnical Engineering Division* 107(GT8): 1129-1149.

Niemunis, A. 2003. Extended hypoplastic models for soils. Report No. 34, Institute of Soil Mechanics and Foundation Engineering, Ruhr-University Bochum.

Niemunis, A., Wichtmann, T. & Triantafyllidis, Th. 2003. Compaction of freshly pluviated granulates under uniaxial and multiaxial cyclic loading. In *XIIIth European Conference On Soil Mechanics and Geotechnical Engineering: Geotechnical problems with man-made and man-influenced grounds, Prag*: 855-860.

Niemunis, A., Wichtmann, T. & Triantafyllidis, Th. 2004. Explicit accumulation model for cyclic loading. In *International Conference on Cyclic Behaviour of Soils and Liquefaction Phenomena, Bochum, 31 March - 02 April*. Balkema.

Sawicki, A. & Świdzi´nski, W. 1987. Compaction curve as one of basic characteristics of granular soils. In E. Flavigny & D. Cordary (ed.), *4th Colloque Franco-Polonais de Mechanique des Sols Appliquee, Grenoble*, 1: 103-115.

Sawicki, A. & Świdzi´nski, W. 1989. Mechanics of a sandy subsoil subjected to cyclic loadings. *International Jounal for Numerical and Analytical Methods in Geomechanics* 13: 511-529.

Suiker, A.S.J. 1999. Static and cyclic loading experiments on non-cohesive granular materials. Report No. 1-99-DUT-1, TU Delft.

Triantafyllidis, Th., Wichtmann, T. & Niemunis, A. 2003. Explicit accumulation model for granular materials under multiaxial cyclic loading. In *6th International Workshop On Mathematical Methods In Scattering Theory and Biomechanical Engineering, Ioannina*. World Scientifi c.

Triantafyllidis, Th., Wichtmann, T. & Niemunis, A. 2004. On the determination of cyclic strain history. In *International Conference on Cyclic Behaviour of Soils and Liquefaction Phenomena, Bochum, 31 March - 02 April*. Balkema.

Wichtmann, T., Niemunis, A. & Triantafyllidis, Th. 2004a. Accumulation of strain in sand due to cyclic loading under drained triaxial conditions. *Soils & Foundations (submitted)*.

Wichtmann, T., Niemunis, A. & Triantafyllidis, Th. 2004b. The effect of volumetric and out-of-phase cyclic loading on strain accumulation. In *International Conference on Cyclic Behaviour of Soils and Liquefaction Phenomena, Bochum, 31 March - 02 April*. Balkema.

Wichtmann, T. & Triantafyllidis, Th. 2004a. Influence of a cyclic and dynamic loading history on dynamic properties of dry sand, part I: cyclic and dynamic torsional prestraining. *Soil Dynamics and Earthquake Engineering (accepted)*.

Wichtmann, T. & Triantafyllidis, Th. 2004b. Influence of a cyclic and dynamic loading history on dynamic properties of dry sand, part II: cyclic axial preloading. *Soil Dynamics and Earthquake Engineering (accepted)*.

Youd, T.L. 1972. Compaction of sands by repeated shear straining. *Journal of the Soil Mechanics and Foundations Division* 98(SM7): 709-725.